IAC-11-D1.1.9

Geo-engineering Using Dust Grains in Heliotropic Elliptical Orbits

Bewick, R.*, Lücking, C., Colombo, C., Sanchez, J.P., McInnes, C.R.
Advanced Space Concepts Laboratory, University of Strathclyde
Glasgow, G1 1XJ, United Kingdom

This paper examines the concept of a Saturn-like Earth ring comprised of dust grains to offset global warming. A new family of non-Keplerian periodic orbits, under the effects of solar radiation pressure and the Earth's oblateness J_2 perturbation, is selected to increase the lifetime of the passive cloud of particles and, thus, increase the efficiency of this geo-engineering strategy. An analytical model is used to predict the evolution of the dust due to solar-radiation pressure and the J_2 effect. The attenuation of the solar radiation can then be calculated from the ring model. In comparison to circular orbits, eccentric orbits yield a more stable environment for small grain sizes and therefore achieve higher efficiencies when the orbital decay of the material is considered. Moreover, the special orbital dynamics experienced by high area-to-mass ratio objects, influenced by solar radiation pressure and the J_2 effect, ensure the ring will maintain a permanent heliotropic shape, with dust spending the largest portion of time on the Sun facing side. It is envisaged that small dust grains can be released with an initial Δv to enter an eccentric orbit with Sun-facing apogee. Finally, an estimate of 5.94×10^{11} kg is computed as the total mass required to offset the effects of global warming.

NOTATION

a	semi-major axis [m]
a_f	semi-major axis of the feeder orbit [m]
a_g	semi-major axis of the generator orbit [m]
a_{SRP}	acceleration by solar radiation pressure [m/s^2]
e	eccentricity
e_0	equilibrium eccentricity
e_{crit}	critical eccentricity
e_f	eccentricity of the feeder orbit
f	true anomaly [rad]
$F_\odot$	solar flux [W/m^2]
H	Hamiltonian
h_{peri}	altitude of the perigee [m]
J_2	second order zonal harmonic coefficient
$n_\odot$	rotational rate of the Earth around the Sun [rad/s]
r	grain radius [m]
R	radial distance from centre of the Earth [m]
R_E	radius of the Earth [m]
α	solar radiation pressure parameter
δ	density of asteroid dust [kg/m^3]
κ	J_2 effect parameter
Λ	attenuation coefficient [m^{-1}]
$\lambda_\odot$	angle of position of the Sun on the ecliptic with respect to the vernal equinox [rad]
μ	gravitational parameter of the Earth
ϕ	solar radiation – perigee – angle [rad]
θ	solar radiation – orbital position – angle [rad]

1. INTRODUCTION

The current consensus within the scientific community is that climate change is not only happening but is almost unavoidable. Projections made using climate models over recent years have suggested that the mean global temperature is likely to increase by 1.1°C to 6.4°C by the end of this century [1]. With the continuing industrialisation of the developing world and the lack of a legally binding international protocol on the tackling of global greenhouse gas emissions, this temperature increase seems likely to happen. While the focus of international efforts should remain with the attempts to prevent climate change by the reduction of greenhouse gas emissions, it is prudent to investigate methods to mitigate its effects. This can be achieved by the deliberate manipulation of the Earth's climate, commonly referred to as climate engineering or geo-engineering.

Several proposals for possible geo-engineering methods have been made and these can generally be placed in two categories; solar radiation management and carbon sequestration [2]. Solar radiation management focuses on the reduction of the amount of sunlight being absorbed by the Earth's atmosphere, by either increasing the Earth's albedo, for example through using reflective roofing materials, or by reducing the level of sunlight reaching the surface, for example by placing aerosol particles into the stratosphere to reflect sunlight. Alternatively carbon capture techniques aim to deal with the fundamental cause of global warming, an excess of greenhouse gases in the atmosphere, by either direct or indirect methods. Direct methods include capturing

* russell.bewick@strath.ac.uk

CO_2 from the air and placing it into storage, whilst an indirect method is the fertilisation of the ocean to stimulate increased algal growth, with these algae then leading to increased CO_2 uptake.

A report into geo-engineering conducted by the Royal Society in 2009 [2] examines the feasibility of all types of schemes based on the criteria of effectiveness, affordability, timeliness and safety. In general the report appears to show that there is no perfect solution, with the schemes that appear most effective suffering in other criteria such as affordability. One of the most effective solutions suggested is the use of space-based solar reflectors to reduce incident solar insolation. Whilst this technique does not appear to be affordable or timely, it does have a key advantage over other schemes; neither the Earth's surface nor atmosphere needs to be physically changed. This is a significant benefit as it reduces the grounds for ethical objections based on the uncertain nature of many geo-engineering proposals. As an example, the injection of SO_2 particles into the stratosphere is rated as having low safety in the Royal Society report. This is because there are indications, from observations of volcanic eruptions, that an increased sulphate concentration in the stratosphere could have adverse effects on the hydrological cycle and ozone layers [2]. Space-based geo-engineering will avoid the risks associated with these types of schemes, though there may yet be side effects that cannot be predicted.

It has been estimated that in order to offset the effects of global warming caused by a doubling of the CO_2 concentration (compared to pre-industrial levels and corresponding to an increase in global temperature of approximately 2°C) solar insolation must be reduced by 1.7% [3]. Similarly for a quadrupling of CO_2 the required insolation change is 3.6% [4].

There have been several different proposals to date regarding the reduction of solar insolation using space-based methods, the key characteristics of which can be seen in Table 1. The methods either utilise a cloud of dust [5-7] or solid reflectors or refractors [5-7] to reduce the level of solar insolation. Typically the methods that require the least mass are those that use solid reflectors/refractors whilst the mass for dust cloud methods are orders of magnitude higher. This is mostly due to the increased level of control that can be placed upon the solid reflectors, hence they can be stationed in optimum positions. Dust clouds cannot be controlled and can only be placed with suitable initial conditions, with subsequent replenishment necessary due to the orbital decay or perturbation of the particle orbits. Conflicting with this, though, is the consideration of the engineering complexity of the system. Whilst dust clouds are a relatively crude method, the material can be readily produced with little processing, whereas solid reflectors must either be manufactured terrestrially, and then launched into position, or manufactured in-situ. Clearly taking this into account, the low rating for affordability and timeliness indicated in the Royal Society report can be understood.

A key factor that affects the relative mass of the different methods is the amount of time that the reflectors or dust spends along the Sun-Earth line. For example the method proposed in [5, 8-11] to place clouds of dust at the L_4/L_5 Lagrange points of the Earth-Moon system has a clear benefit as these points are passively stable. However, as these points effectively orbit around the Earth they are only occasionally in a position to reduce solar insolation. Furthermore, the movement of the clouds will create a flickering effect. On most occasions there will be no change in insolation whilst at those times when the cloud is present the insolation change required will be much greater than the net 1.7% reduction.

The work presented in this paper aims to investigate further the feasibility of using a Saturn-like ring around the Earth in the equatorial plane, as first suggested in [6]. The difference between the approach presented in [5] and this paper is that a more thorough consideration of the orbital mechanics of the high area-to-mass ratio dust grains is used, including solar radiation pressure (SRP) and the effect of Earth's oblateness, the J_2 effect. Subsequently it will be shown that solar radiation pressure has a large effect on the orbital evolution of small dust particles. Small particles, for instance, are more mass efficient at intercepting solar photons, i.e. they have a higher area-to-mass ratio, but at the same time they are also more prone to be affected by perturbative forces, and thus more likely to deorbit. Grains with the sizes and at the altitudes suggested in [5] will deorbit rapidly as will be shown in a later section. A balance between mass efficiency and orbital stability must therefore be found.

Position	Method	Insolation Change [%]	Required Mass [kg]	Ref.
Earth orbit	Dust ring	1.6	$2.3\text{x}10^{12}$	[5]
Earth orbit	Solar reflector	1.6	$5.0\text{x}10^{9}$	[5]
Earth-Moon L_4/L_5	Dust Cloud	1.4	$2.1\text{x}10^{14}$	[5]
Sun-Earth L_1	Solar Reflector	1.8	$2.6\text{x}10^{11}$	[6]
Sun-Earth L_1	Solar Refractor	1.8	$2.0\text{x}10^{10}$	[8]
Sun-Earth L_1	Dust Cloud	1.7	$1.9\text{x}10^{10}$	[11]

Table 1: Key properties of the different geo-engineering methods proposed in literature.

2. ORBITAL DYNAMICS

2.1 Hamiltonian model of the orbital dynamics

In order to tackle the problem analytically, a simplified planar model is used. We are considering the orbit in a rotational reference frame that follows the Earth around the Sun. In this frame three parameters are needed to define any in-plane orbit. The eccentricity e, semi-major axis a and the angle between the direction of the solar radiation and the radius of the perigee with respect to the Earth, ϕ. The position of the dust grain is also defined with respect to the direction of the sunlight using the angle θ, where $\theta = \phi + f$ with true anomaly f. Figure 2 shows the geometry of the rotational reference frame.

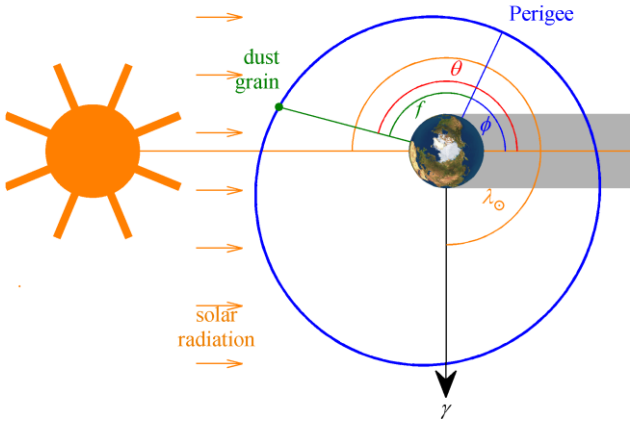

Figure 1: Geometry of an in-plane orbit in the rotational reference frame

Krivov and Getino's work on the orbital dynamics of high area-to-mass ratio spacecraft introduces an approximate Hamiltonian for planar obits under the effects of solar radiation pressure and the Earth's oblateness [7]. This analytical model does not consider eclipses and the tilt of the Earth's rotational axis with respect to the ecliptic plane. As a consequence, the semi-major axis remains constant and the evolution of the orbit can be described only by its eccentricity *e*, defining the changing shape of the orbit, and solar radiation perigee angle ϕ, defining the orientation. The change of orbital elements due to solar radiation pressure and J_2 with respect to the progression of the angle between the position of the Sun on the ecliptic with respect to the vernal equinox, $\lambda_\odot$, is:

$$\frac{de}{d\lambda_\odot} = -\alpha\sqrt{1-e^2}\sin\phi \qquad (1)$$

$$\frac{d\phi}{d\lambda_\odot} = -\alpha\frac{\sqrt{1-e^2}}{e}\cos\phi + \kappa\frac{1}{(1-e^2)^3} - 1 \qquad (2)$$

where α is the radiation pressure parameter and κ the J_2 effect parameter, calculated as:

$$\alpha = \frac{3}{2n_\odot}a_{SRP}\sqrt{\frac{a}{\mu}} \qquad (3)$$

$$\kappa = \frac{3}{2}\frac{}{n_\odot} J_2 \; R_E{}^2\sqrt{\frac{\mu}{a^7}} \qquad (4)$$

where μ is the gravitational parameter of the Earth, J_2 its second order zonal harmonic coefficient, R_E its radius and $n_\odot$ the rate of rotation of the Earth around the Sun. While κ is only a function of the semi-major axis, α is also dependent on a_{SRP}, the acceleration received from solar radiation pressure (SRP). For circular objects with radius *r* and density δ it can be calculated as follows:

$$a_{SRP} = \frac{F_\odot}{c}\frac{4}{3\delta r} \qquad (5)$$

where $F_\odot$ is the solar flux and *c* is the speed of light.

The resulting Hamiltonian is [12]:

$$H = -\sqrt{1-e^2} + \alpha\, e\cos\phi - \frac{\kappa}{3\sqrt{1-e^2}^3} \qquad (6)$$

The phase space has an equilibrium e_0 at $\phi = 0$. These orbits are frozen with their apogee pointing towards the Sun and are therefore called heliotropic orbits. For $\alpha = 0$, i.e. without the effect of SRP this equilibrium corresponds to an orbit with a frozen orientation towards the Sun [12]. This eccentricity is the minimum boundary value for the equilibrium eccentricity e_0 at a given semi-major axis since the equilibrium eccentricity increases with area-to-mass ratio. Figure 2 shows $\min(e_0)$ as a function of semi-major axis. In the background a gradient shows the height of perigee with $h_{peri} = 0$ km and $h_{peri} = 2000$ km specifically marked. 2000 km is approximately the altitude from which the effect of drag on the orbital evolution is negligible, even for very high area-to-mass ratios [13, 14]. A ring of dust at or beyond this distance from the Earth will remain in place quasi infinitely. It can be seen from the figure that heliotropic orbits do not exist above c. 16,000 km semi-major axis. Above c. 13,500 km semi-major axis they become unstable due to drag.

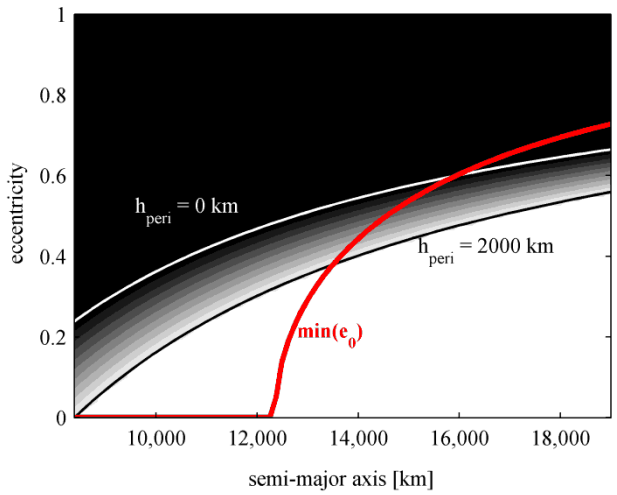

Figure 2: Minimum eccentricity (α = 0) of the heliotropic equilibrium orbit min(e_0) as a function of semi-major axis. The gradient in the background corresponds to the height of the perigee of the corresponding orbit with h_{peri} = 0 km and h_{peri} = 2000 km specifically marked, where the effect of drag is non-negligible.

2.2 In-plane orbital evolution of dust

As explained above, a smaller grain size is desirable as the mass efficiency of the geo-engineering measure is inversely proportional to grain radius. If a grain with a specific area-to-mass ratio is released in any orbit its orbit will then evolve by librating or rotating around its equilibrium eccentricity. The greater the initial distance from the libration point in the phase space the larger the maximum eccentricity reachable. Therefore it is more efficient to release the dust grains at a higher initial eccentricity to prevent them from de-orbiting due to drag. Figure 3 compares the orbital evolution of grains with different radii when they are released in a circular and elliptical orbit with the same semi-major axis. A grey colour marks the area in which the orbits will experience drag and we consider grains which pass through this area "lost". It can be seen that while for an initially circular orbit all grains with a radius smaller than 13 microns will be lost (see Figure 3a), in the elliptical case grains as small as 6.5 microns survive (see Figure 3b). It follows that release at the critical eccentricity yields the best results and that the smallest possible grain radius at any semi-major axis is the one which has its equilibrium point at the critical eccentricity.

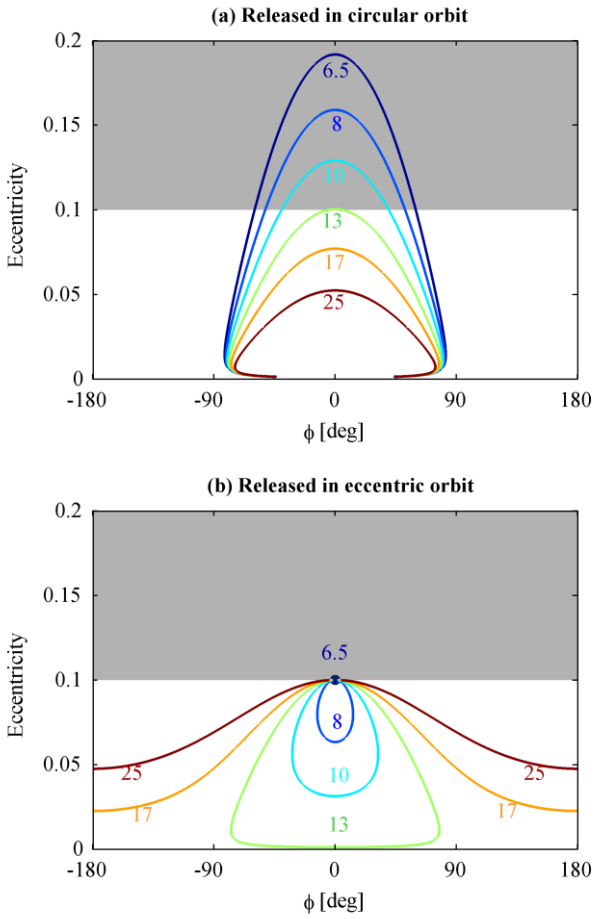

Figure 3: Orbital evolution in the *e*-ϕ phase space for grains with different radii from 6.5 to 25 microns released at c. 9300 km semi-major axis with e = 0 (a) and e = e_{crit} (b). The grey zone marks the area in which the perigee of the orbit is closer than 2000 km to the surface of the Earth.

2.3 Choice of feeder orbit

We can determine the smallest possible grain radius as a function of semi-major axis by finding the particle radius for which the equilibrium eccentricity e_0 is equal to e_{crit}, the critical eccentricity corresponding to the smallest allowable perigee height h_{peri}. To find the minimum particle radius we set $\phi = 0$ in Eq. (2), set $\frac{d\phi}{d\lambda_\odot}$ equal to zero, substitute e with $e_{crit} = 1 - \frac{R_E + \min(h_{peri})}{a}$, solve for α and combine with Eqs. (3) and (5) to get:

$$r_{\min} = \frac{2F_\odot}{cn_\odot \delta}\sqrt{\frac{a}{\mu}}\frac{\sqrt{1-e_{crit}^{\ 2}}^{5}}{e_{crit}(\kappa(a)-(1-e_{crit}^{\ 2})^2)} \qquad (7)$$

The density δ for the asteroid grains can be approximated to 3500 kg m^{-3} [15].

Another measure of the efficiency of a ring for geo-engineering is how much of its orbital period a grain spends blocking solar radiation. This is dependent on the orbital geometry and takes into account that a grain travels slower at apogee than at perigee. We call the resulting percentage (of time spent in the useful region) geometrical efficiency which can be found numerically.

Using these indicators of efficiency we can next choose the semi-major axis likely to be most efficient for geo-engineering. Figure 4 shows the dust grain minimum radius and the geometrical efficiency of a circular orbit and an orbit with $e = e_{crit}$ over semi-major axis. Both the circular and elliptical orbit are considered because we will be releasing grains with a distribution of radii and not all of these have an equilibrium at the critical eccentricity. A good compromise between low minimum grain size and high geometrical efficiency is desired. Considering the results in Figure 4, an advantageous initial orbit for the dust ring, referred thereafter as the feeder orbit, has a semi-major axis of a_f = 9318 km and an eccentricity of $e_f = 0.1$. Its apogee is Sun-pointing.

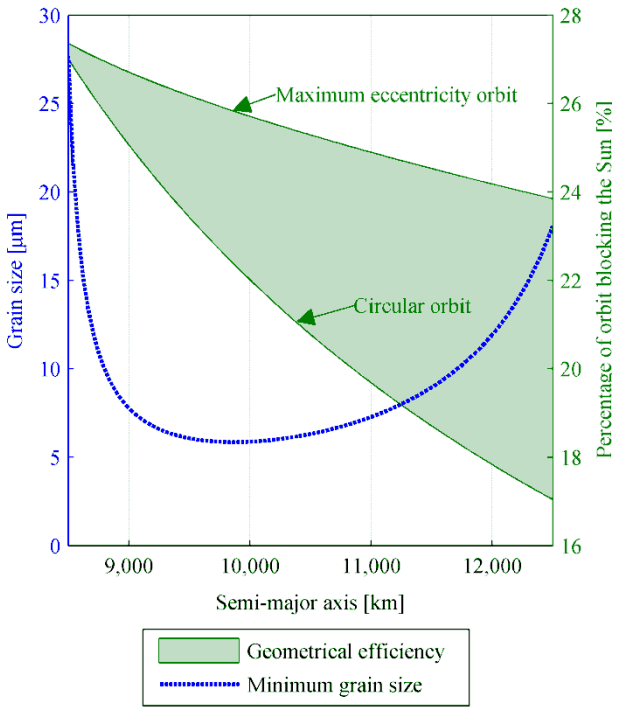

Figure 4: Geo-engineering efficiency indicators (grain size and orbit geometry) over semi-major axis. The geometrical efficiency is given as a range from a circular orbit to an orbit with critical eccentricity and Sun-pointing apogee.

2.4 3D orbital evolution of dust

The actual evolution of dust particles differs from the one predicted by the Hamiltonian in Eq. (6) because of the 23.5 degree tilt angle of the equator with respect to the ecliptic plane. As a consequence, a dust ring initially positioned on the ecliptic plane will be subject to a nodal drift, due to the effect of J_2 and SRP and out of plane oscillations under solar radiation pressure. As analysed in [16], the simplified 2D phase space approximation used in Section 2 maintains its structure for small tilt angle (less than 30 degree as in the Earth case) and small inclinations. Figure 5 represents the 3D evolution of the ring over a period of 20 years, propagated through a set of non-singular Lagrangian elements derived by Krivov [17] (The effect of eclipses is neglected). The harmonic oscillation in the e-ϕ phase space is still recognisable, although the single line for a given area-to-mass ratio extends to a band (see Figure 5a). Note that in the 3D case the solar radiation perigee angle ϕ needs to be defined as

$$\phi = \Omega + \omega - \left(\lambda_{\odot} - \pi\right)$$

where Ω and ω are respectively the argument of the ascending node (counted from the vernal equinox) and the argument of perigee of the grain's orbit, and $\lambda_{\odot}$ defines the true longitude of the Sun on the ecliptic.

A full characterisation of the Earth's ring is given when we consider also the perturbations to the inclination and the ascending node, which describes the vertical structure (see Figure 5b). The dust grains display complex inclination traces, however the magnitude of the inclination changes are limited to 0.2 degree for the smallest grains as shown in Figure 6. The apogee point of the heliotropic orbits will oscillate below and above the ecliptic plane as shown in Figure 7 which represents the declination of the apogee with respect to the ecliptic as seen from the Sun. This angle oscillates approximately between -23.7 and 23.7 degrees depending on the season and the change in inclination.

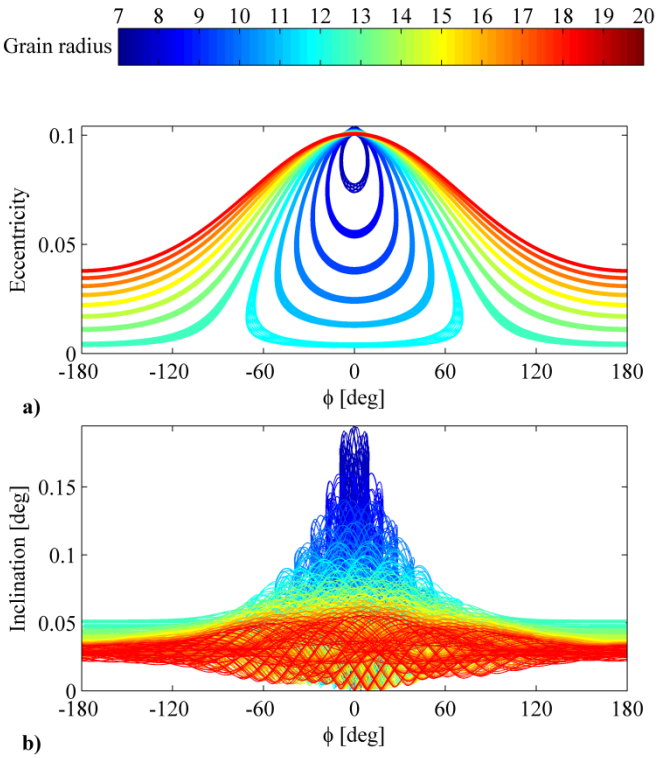

Figure 5: 3D evolution of the dust ring over a period of 20 years. a) Planar structure in the ϕ-e phase space and b) vertical structure in the ϕ-i phase space.

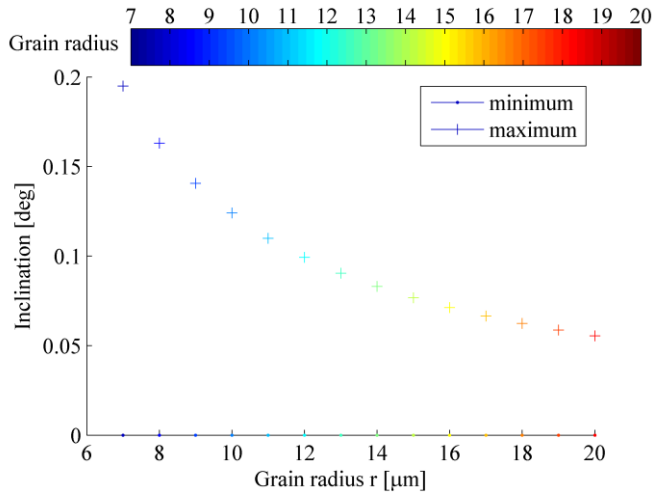

Figure 6: Maximum (cross) and minimum (dot) inclination change on the equator as function of the grain radius.

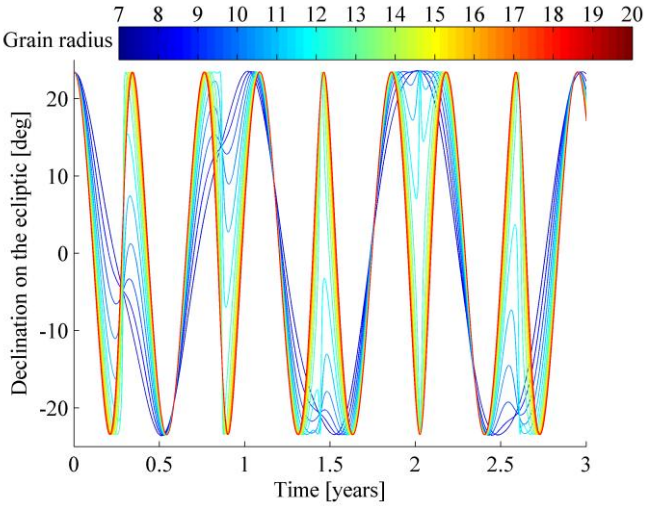

Figure 7: Declination of the apogee point of the grains' orbits with respect to the Sun.

3. MISSION SCENARIO

3.1 Dust source

Some consideration must be given to the source of dust that is to be dispersed from the feeder orbit as it is likely that a large amount is required. Previous geo-engineering concepts have suggested the use of dust sourced from the Earth, Moon, asteroids and comets [18]. It has been shown that the amount of asteroid material that can be captured into a weakly bound Earth orbit with a threshold velocity lower than that of lunar escape velocity, 2.37 km s^{-1}, is $6x10^{13}$ kg [5-7]. For the material required in this geo-engineering scenario an extra velocity increment of 2.7 km s^{-1} would be required to lower the orbit to the position of the feeder orbit therefore doubling the velocity requirement.

Despite the additional costs of transporting asteroid material to medium Earth orbit, the use of captured asteroid resources would still be more efficient than lifting material off the surface of the Earth. This also applies for schemes that require solid reflectors to block solar radiation where large devices must be manufactured and then launched into the correct position. Lifting such large masses is beyond current launch capabilities. Using asteroid material rather than lunar dust has the added benefit that the material can be mined and ground to finer grain sizes, if required, whilst in the feeder orbit before being released, thus decreasing the need for large numbers of spacecraft to ferry material from the Moon.

An additional source of material could possibly be spent rocket stages and other debris that can be ground up to dust. The NORAD database of tracked space objects reveals that there are over 1,000 spent rocket stages and over 10,000 pieces of other debris in LEO and MEO orbits. Assuming a

minimum mass of 1 metric tonne per rocket stage gives a lower bound of $1x10^6$ kg in this region. This is a relatively small amount of material in comparison to the scale of typical geo-engineering schemes but would never-the-less be useful. Using this material has the added advantage of "tidying up" the space environment.

The asteroid is envisaged to be captured into a circular, equatorial generator orbit with a_g = 10,000 km semi-major axis (see Figure 8). It follows that 10,000 km is also the radius of the apogee for the feeder orbit selected in the previous section. Since the area-to-mass ratio of an asteroid is very small, the effect of solar radiation pressure is negligible. The orbit is thus unperturbed.

The dust grains will be continuously extracted from the asteroid, milled to achieve a certain radii distribution and collected during one orbit. Whenever the generator passes $\theta = \pi$ it ejects the collected dust with the correct Δv to inject it into the feeder orbit using a mass driver. From this feeder orbit the grains will then evolve and spread due to their different area-to-mass ratios and thus form the dust ring. Because the period of the generator orbit and the feeder orbit are different, after a while grains will be distributed at all positions in the orbit. After a maximum of one year all positions on the libration curves in the phase space will be filled and after 4 years the orbits will be spread over all inclinations smaller than 0.2 degree with respect to the equator. Figure 8 shows a scale illustration of the mission concept.

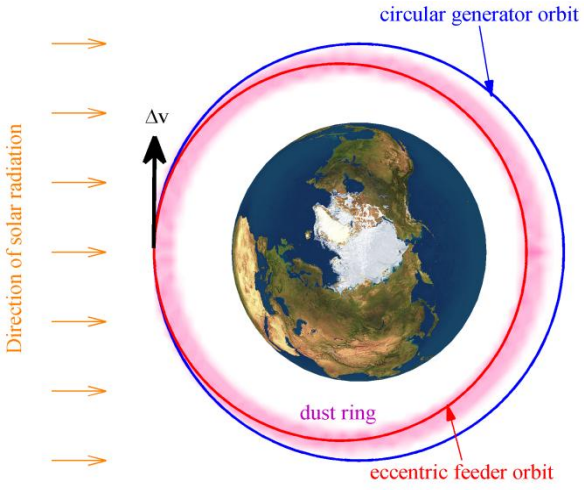

Figure 8: Illustration of the mission concept with generator orbit, feeder orbit and the resulting dust ring.

3.2 Dust grain size distributions

The milled dust is assumed to be distributed log-normally in grain radius:

$$f_{\mu,\sigma}(x) = \frac{1}{x\sigma\sqrt{2\pi}} e^{-\frac{(\ln x - \mu)^2}{2\sigma^2}} \quad (8)$$

Three possible distributions have been chosen. D1 is an optimistic guess with small mean and low standard deviation. D2 is a realistic distribution and achievable with existing terrestrial milling machinery[1,2]. D3 is a pessimistic guess with high mean and large standard deviation. Table 2 shows the chosen values for mean and standard deviation and Figure 9 shows the three distributions as probability density functions.

Distribution	Mean μ	Standard deviation σ
D1	–11.5	0.1
D2	–11.35	0.15
D3	–11.2	0.25

Table 2: Values for mean and standard deviation of the three dust grain distributions.

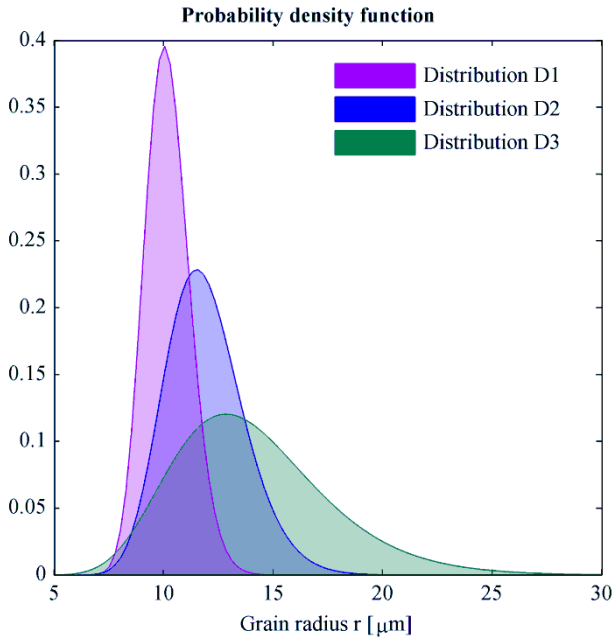

Figure 9: Probability density functions for the three distributions of grain radii considered.

[1] http://www.zenithcrusher.com/ Last accessed 05 Sep 2011
[2] http://www.crushermills.com/ Last accessed 05 Sep 2011

4. RING MODEL

To derive the mass needed for an average insolation reduction of 1.7% over one year the attenuation through the ring must be known. This is achieved by using the Beer-Lambert law;

$$I = I_0 e^{-\Lambda l} \tag{9}$$

where I_0 is the solar constant before passing through the ring, Λ is the attenuation coefficient and l is the path length . The attenuation coefficient at any given point is calculated by;

$$\Lambda = \int_{r_1}^{r_2} \pi r^2 \rho(r) dr \tag{10}$$

where r is the grain radius and $\rho(r)$ is the number density of grains at each radius. Since the attenuation coefficient is likely to change through the ring, the attenuation coefficient must be integrated over the path length and hence Eq. (8) becomes;

$$I = I_0 e^{-\int_0^l \Lambda(l) dl} \tag{11}$$

To determine the attenuation coefficient for the different distributions a phase space density model must to be built. To achieve this a two dimensional model of the ring will be constructed, neglecting the tilt of the Earth's rotational axis. The attenuation coefficient is then calculated for this in-plane orbit. Then the orbital plane is tilted with respect to the ecliptic plane and the inclination change added.

4.1 In-plane model

An expression is needed to find the radius of a grain passing through any point (ϕ, e) in the phase space. This can be derived by setting the Hamiltonian Eq. (6) with (ϕ, e) equal to the Hamiltonian of the feeder orbit with $(0, e_f)$ and solving for α . Then applying Eqs. (3) and (5), gives:

$$r(\phi, e) = \frac{\dfrac{6F_\odot}{cn_\odot \delta}\sqrt{\dfrac{a}{\mu}}(e_f - e\cos\phi)}{3\left(\sqrt{1-e_f^{\,2}} - \sqrt{1-e^2}\right) + \kappa\left(\dfrac{1}{\sqrt{1-e_f^{\,2}}^{\,3}} - \dfrac{1}{\sqrt{1-e^2}^{\,3}}\right)} \tag{12}$$

The probability of finding any grain in a differential element around a given (ϕ, e) in the phase space can then be determined. This is achieved by calculating the required radius of the grain using Eq. (12). From this the probability of a grain having this radius can be found with the probability density function. Together with its specific density at the considered location in the phase space this gives the desired combined probability. The specific density is found numerically by first calculating the time a grain of the given size needs to complete one full libration in the phase space. Then this figure is compared with the evolution velocity at the given position calculated using Eqs. (1) and (2). Figure 10 shows the resulting number density in the phase space for the three distributions of grain radii introduced in the previous section. It is shown relative to the average number density in the phase space. As expected the highest density can be found in the release position, the feeder orbit, at $(0, e_f)$. The slimmest distribution, D1, shows high density in higher eccentricity orbits with the apogee facing within about 45 degrees of the Sun. The wider the grain size distribution the more dispersed the dust cloud is in the phase space. It can be assumed that the slimmest distribution has the most grains blocking sunlight. To ascertain this assumption the dust density around the Earth in polar coordinates is calculated next.

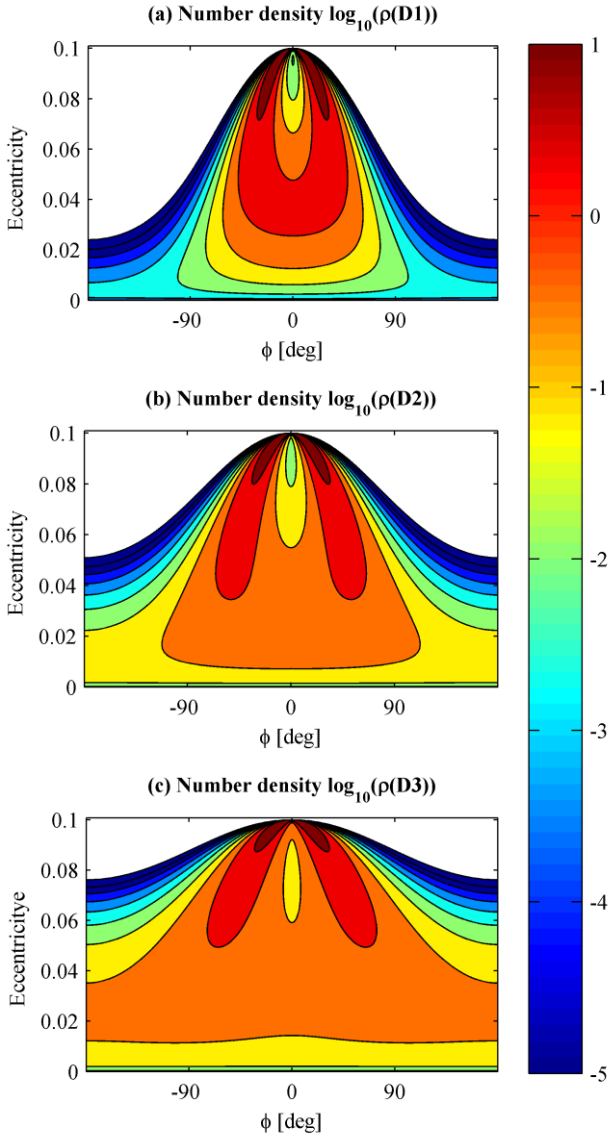

Figure 10: Number density relative to average number density in the phase space for different grain radius distributions.

The polar coordinate system chosen is a rotational reference frame with fixed orientation towards the sun. Any position in the orbital plane is determined by R, the distance to the centre of the Earth, and θ, the angle with respect to the direction of solar radiation as shown in Figure 1.

Figure 11 shows the accumulated in-plane number density as a function of θ for the three different initial distributions. It can be seen that the slimmest distribution D1 indeed has the largest number of particles facing the sun, about 15% more than the orbit average.

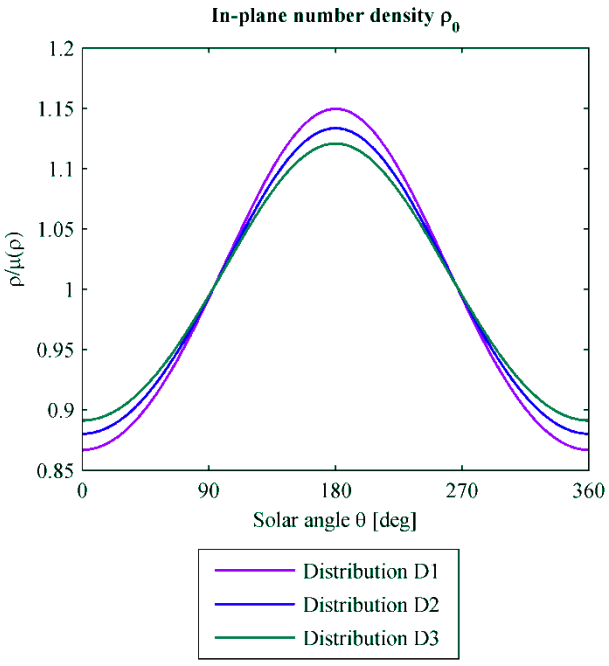

Figure 11: Sum of the in-plane number density for different solar angles θ in relation to the average.

The in-plane number density, which is the probability of finding a grain in a given area of the orbital plane, can then be used to calculate Λ_0, the in-plane attenuation coefficient, using Eq.(10). The in-plane coefficient differs from the final value to be used as here the number density is in terms of area not volume and hence there is an intermediate step to calculate the true attenuation coefficient.

Figure 12 shows the in-plane attenuation coefficient relative to the maximum attenuation for the three different distributions. The maximum attenuation occurs predictably at the intersection with the generator orbit at $\theta = \pi$ and $R = a_f(1+e_f)$. The feeder orbit itself can also be seen in all three figures. Apart from the feeder orbit, a wider dust ring is distinctly discernible in all three figures with attenuation values of around 10% of the maximum. The slimmest distribution D1 has the narrowest ring measuring approximately 600 km. The ring of the widest distribution D3 is about twice as wide at approximately 1200 km. Although distribution D1 is favourable because of its small average grain radius and its higher geometrical efficiency, D3 could have an advantage with the wider ring allowing the burden of the reduced insolation to be stretched over a larger area of the Earth, thus making the shadowing effect less harsh.

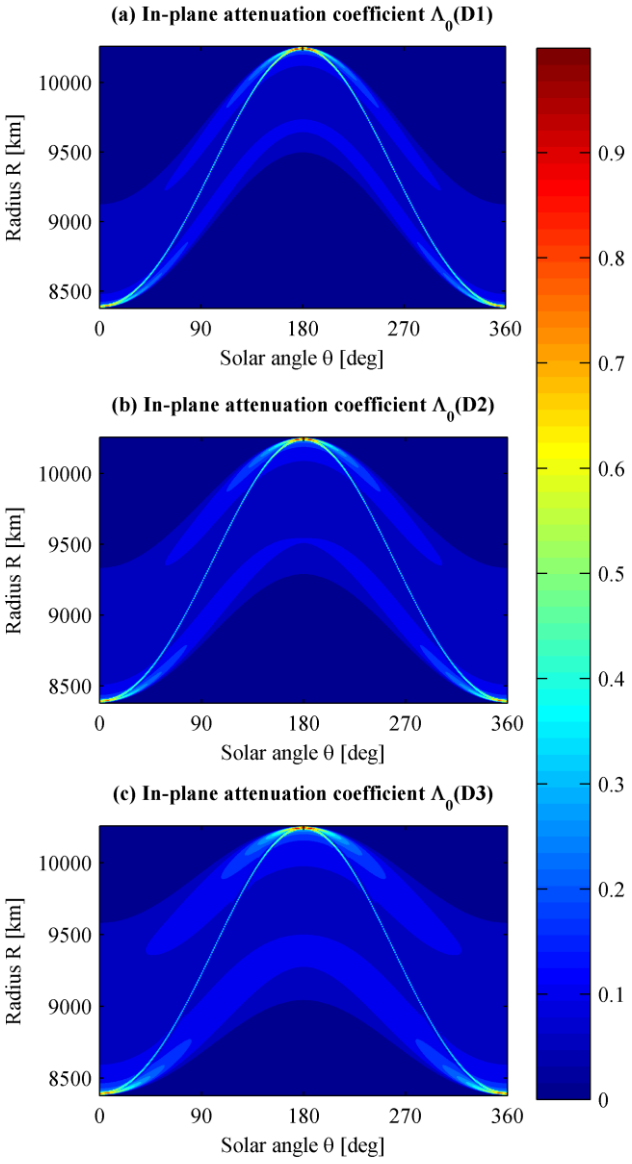

Figure 12: In-plane attenuation coefficient in polar coordinates and in relation to the maximum attenuation.

4.2 Three dimensional model

To fully determine the mass of dust required to offset the 1.7% insolation change a 3D model of the ring must be constructed. The first stage in this process is to transfer the in-plane attenuation coefficient into a three dimensional attenuation coefficient. This is estimated by dividing the in-plane coefficient by the out of plane width at radius R;

$$\Lambda(R,\theta) = \frac{\Lambda_0(R,\theta)}{2R\delta i} \tag{13}$$

To construct the 3D model it is assumed that as the distance between the ring and the Earth is small in comparison to the distance to the Sun, the solid angle that it subtends will have a negligible effect on the results of this paper. Therefore the solar insolation can be assumed to be travelling as a plane wave. Hence, the overall attenuation over the Earth's surface shall be determined by integrating along the x-axis for given values of y and z.

The geometry of the problem can be seen in Figure 13. For a given inclination of the ring to the Sun line the exit and entry points of the integration line can be calculated and the Beer-Lambert law can be applied between these two positions. For each point along the integration line the position must be transformed from Cartesian coordinates to the (R,θ) system that describes the attenuation coefficient. This value can then be multiplied by the path length to give the fractional intensity before being integrated.

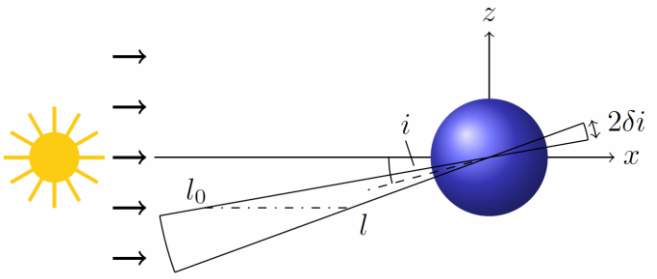

Figure 13: Diagram of the 3D ring model (northern summer pictured).

To find an accurate determination of the mass required, this process must be averaged over time. This is necessary as the angle between the equatorial and ecliptic planes, from the viewpoint of the sun, will change over the course of a year. It can be found that the inclination angle between the Sun-line and the equatorial plane is described by a *sin* function, assuming the starting point is at the northern hemispheres spring. The view of the Earth, as seen from the Sun, is shown in Figure 14 for different times of the year. Next the mass required for the three different dust distributions can be found.

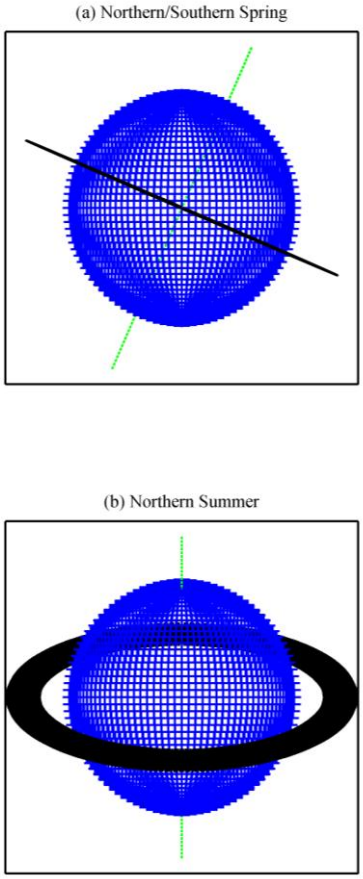

Figure 14: Impression of the view of the Earth as seen from the Sun for the spring (a) and summer in the northern hemisphere (b).

5. RESULTS

The mass required for each of the dust distributions described previously can be seen in Figure 15. It can be seen, as would at first be expected, that the distribution with the greatest fraction of its number density along the Sun line requires the lowest mass of $5.94\text{x}10^{11}$ kg. This is additionally due to the smaller grain sizes leading to greater efficiency. It is noteworthy that the difference between the D1 and D2 distributions is considerably smaller than the difference to the D3 distribution. A large amount of this difference will be due to the increase in grain size, however it was expected that the increased spread seen in Figure 9 would partially offset this decreased efficiency, as is the case between D1 and D2. This increased spread is particularly useful at increased inclinations as it spreads the insolation change away from being a very narrow band to a slightly wider band.

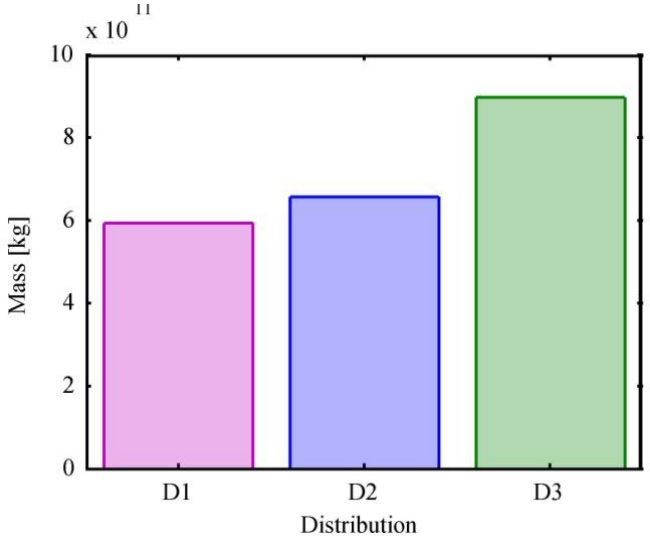

Figure 15: Mass required to give an average 1.7% insolation change for three dust distributions.

All the masses calculated in this paper are lower than the value of 2.3×10^{12} kg seen in [19]. This is in large part due to the inclusion of the effects of solar radiation pressure and the J_2 effect and their use to find heliotropic ring patterns that will be long-lived. This is essential for the success of such a proposal as the length of time that such a scheme must be in place cannot be known and would depend on many factors related to our tackling of global warming.

The insolation change as a function of time can be seen in Figure 16. It shows that the insolation change is highly variable with a wide, flat peak greater than the 1.7% required but depressions as low as 0.5%. These depressions occur during spring and autumn where the inclination of the equatorial to ecliptic plane is low. During these phases the view of the ring, as seen in Figure 14, is reduced to $2\delta i R_{max}$ at its maximum.

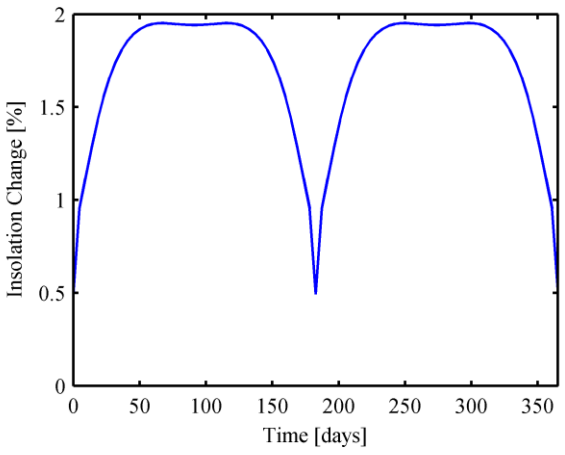

Figure 16: Variation in insolation over the course of a year, giving an average of 1.7%.

Also of interest is the knowledge of where the insolation change over the Earth's surface will be greatest. An analysis of this can be seen in Figure 17. Clearly the greatest effect will be felt in the tropics but particularly closer to the tropical boundaries rather than the equator itself. Additionally it can be seen in Figure 14 that each hemisphere experiences the greatest effects during its winter season. The precise effect that this will have on the local climate cannot be determined here.

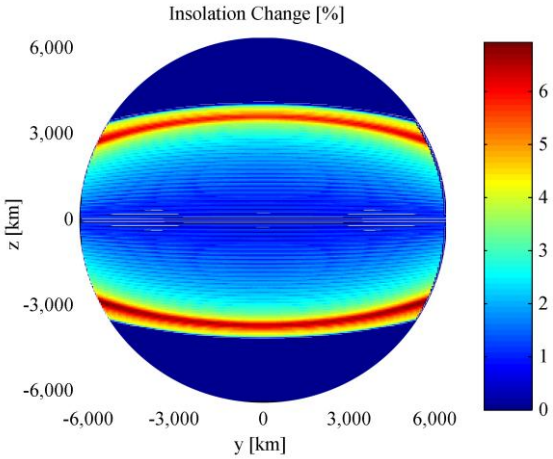

Figure 17: Insolation change over the Earth's surface over the course of a year, as seen from the Sun.

There are other effects that this form of geo-engineering scheme will have on the Earth. As described in [5] the ring will reflect light onto the night side of the Earth, though this effect is small it will amount to several full Moons depending on the inclination of the ring. It will mainly reflect onto the summer hemisphere, possibly leading to increased temperatures. There will also be a danger to spacecraft. The ring will generally inhabit an orbital region above LEO and below the high MEO orbits of the satellite navigation constellations. However, spacecraft and rocket modules in equatorial geostationary transfer orbits (GTO) will pass through the ring and would need protective shielding for this passage higher inclination GTOs avoid the passage however. Also a small fraction, <1%, of very fine grained material will deorbit shortly after injection. These grains have radii of less than 6 microns. They will pass through the busiest region of LEO (< 500 km) quickly because of their very high area-to-mass ratio and thus pose little danger to satellites there. The long lived nature of the greatest part of the rings particles leads to the disadvantage that it cannot easily be removed and that should strong unforeseen side effects occur the measure cannot be abandoned quickly. As a safety feature a scheme would need to be designed to remove the dust, possibly by laser ablation or by using concentrated sunlight.

6. CONCLUSIONS

The concept of a Saturn-like Earth ring comprised of dust grains to offset global warming, first investigated in [5], has been studied from the viewpoint of an increased understanding of the astrodynamics of such small particles. By the inclusion of the perturbations of solar radiation pressure and the J_2 effect the orbital dynamics of these high area-to-mass ratio dust grains has been analysed in the e-ϕ phase space using a Hamiltonian approach. From this analysis stable, sun-pointing orbits have been found that enable a ring to stay in place for long periods of time. Using these orbits as a site for geo-engineering enables an estimate of the mass of dust required to offset a 2°C increase in temperature increase by a 1.7% reduction in solar insolation. The result of this estimate is a dust mass of 5.94×10^{11} kg which is less than the dust cloud methods found in [5] and [5] and of the same order of magnitude as the solid reflector method suggested in [6] but an order of magnitude greater than the refractor method seen in [8]. The use of dust rather than large reflective or refractive devices has the great advantage of reducing the complexity of the system and also, if the dust is sourced from an asteroid, reduces greatly the launch costs of the system. Future work will use more accurate model for taking into account the complex three-dimensional structure of the ring.

ACKNOWLEDGEMENTS

This work was funded by the European Research Council grant 227571 (VISIONSPACE).

REFERENCES

[1] IPCC. "Contribution of Working Groups I, II and III to the Fourth Assessment Report of the Intergovernmental Panel on Climate Change," *Core Writing Team, Pachauri, R.K. and Reisinger, A. (Eds.), IPCC, Geneva, Switzerland. pp 104*, 2007.

[2] Shepherd, J., Caldeira, K., Cox, P., and Haigh, J. "Geoengineering the climate.," *Report of Royal Society working group of geo-engineering*, 2009.

[3] Govindasamy, B., and Caldeira, K. "Geoengineering Earth's radiation balance to mitigate CO_2-induced climate change," *Geophysical Research Letters* Vol. 27, No. 14, 2000, pp. 2141-2144.

[4] Govindasamy, B., Caldeira, K., and Duffy, P. B. "Geoengineering Earth's radiation balance to mitigate climate change from a quadrupling of CO2," *Global and Planetary Change* Vol. 37, No. 1-2, 2003, pp. 157-168.

[5] Pearson, J., Oldson, J., and Levin, E. "Earth rings for planetary environment control," *Acta Astronautica* Vol. 58, No. 1, 2006, pp. 44-57. doi: DOI: 10.1016/j.actaastro.2005.03.071

[6] Struck, C. "The feasibility of shading the greenhouse with dust clouds at the stable lunar Lagrange points," *Journal of the British Interplanetary Society* Vol. 60, No. 3, 2007, pp. 82-89.

[7] Bewick, R., Sanchez, J., and McInnes, C. R. "An L1 positioned dust cloud as an effective method of space-based geo-engineering," *International Astronautical Congress*. Prague, 2010, pp. IAC-10.D1.1.7.

[8] McInnes, C. R. "Space-based geoengineering: challenges and requirements," *Proceedings of the Institution of Mechanical Engineers, Part C: Journal of Mechanical Engineering Science* Vol. 224, No. 3, 2010, pp. 571-580.

[9] Early, J. T. "Space-based Solar Shield to Offset Greenhouse Effect," *JBIS* Vol. 42, No. 12, 1989, pp. 567-569.

[10] Mautner, M. "A Space-based Solar Screen against Climatic Warming," *JBIS* Vol. 44, No. 3, 1991, pp. 135-138.

[11] Angel, R. "Feasibility of cooling the Earth with a cloud of small spacecraft near the inner Lagrange point (L1)," *Proceedings of the National Academy of Sciences* Vol. 103, No. 46, 2006, pp. 17184-17189. doi: 10.1073/pnas.0608163103

[12] Krivov, A. V., and Getino, J. "Orbital evolution of high-altitude balloon satellites," *Astronomy and Astrophysics* Vol. 318, 1997, pp. 308-314.

[13] Driam, J. E., Cefola, P., and Castrel, D. "Elliptical Orbit Constellations - A New Paradigm for Higher Efficiency in Space Systems?," *IEEE Aerospace Conference*. Big Sky, Montana, 2000.

[14] Wertz, J. R. "Coverage, Responsiveness and Accessibility for Various Responsive Orbits," *3rd Responsive Space Conference*. Los Angeles, 2008.

[15] Colombo, C., and McInnes, C. "Orbital dynamics of 'smart dust' devices with solar radiation pressure and drag," *in press Journal of Guidance, Control, and Dynamics*, 2011.

[16] Wilck, M., and Mann, I. "Radiation pressure forces on "typical" interplanetary dust grains," *Planetary and Space Science* Vol. 44, No. 5, 1996, pp. 493-499.

[17] Colombo, C., Lücking, C., and McInnes, C. R. "Orbital Dynamics of High Area-to-Mass Ratio Spacecraft under the Influence of J_2 and Solar Radiation Pressure," *62nd International Astronautical Congress*. Cape Town, 2011.

[18] Krivov, A. V., Sokolov, L. L., and Dikarev, V. V. "Dynamics of Mars-orbiting dust: Effects of light pressure and planetary oblateness," *Celestial Mechanics and Dynamical Astronomy* Vol. 63, No. 3, 1995, pp. 313-339. doi: 10.1007/bf00692293

[19] Sanchez, J. P., and McInnes, C. "Asteroid Resource Map for Near-Earth Space," *Journal of Spacecraft and Rockets* Vol. 48, No. 1, 2011, pp. 153-165.